Low Switching Power Neuromorphic Perovskite Devices with Quick Relearning Functionality

Dani S. Assi, Muhammed P.U. Haris, Vaithinathan Karthikeyan,* Samrana Kazim, Shahzada Ahmad,* and Vellaisamy A. L. Roy*

In the quest to reduce energy consumption, there is a growing demand for technology beyond silicon as electronic materials for neuromorphic artificial intelligence devices. Equipped with the criteria of energy efficiency and excellent adaptability, organohalide perovskites can emulate the characteristics of synaptic functions in the human brain. In this aspect, this study designs and develops $CsFAPbI_3$-based memristive neuromorphic devices that can switch at low power and show larger endurance by adopting the powder engineering methodology. The neuromorphic characteristics of the $CsFAPbI_3$-based devices exhibit an ultra-high paired-pulse facilitation index for an applied electric stimuli pulse. Moreover, the transition from short-term to long-term memory requires ultra-low energy with long relaxation times. The learning and training cycles illustrate that the $CsFAPbI_3$-based devices exhibit faster learning and memorization process owing to their larger carrier lifetime compared to other perovskites. The results provide a pathway to attain low-power neuromorphic devices that are synchronic to the human brain's performance.

1. Introduction

Organohalide perovskites are a promising class of optoelectronic materials with exceptional tunable charge transport behavior that mimics the characteristics of neurons and synaptic functions.[1] These properties make them an excellent choice for neurotrophic and neuromorphic applications. With the potential of being an energy-efficient, scalable, and adaptive neuroelectronic unit for neuromorphic artificial intelligent systems. Organohalide perovskites are the choice of materials to overcome the drawback of

von Neumann architecture.[2] Furthermore, the exponential demand for post-silicon electronic devices in the community, for cost–effective materials with flexible conductance regulation and retention also urges the development of effective materials for artificial synaptic perovskite devices.[3]

Halide perovskites have ABX_3 structure, where A is a monovalent organic cation such as methylammonium and formamidinium, B is a divalent metal cation such as Pb^{2+} or Sn^{2+}, and X is a halide such as Cl^-, Br^- or I^-, has emerged as a potential candidate owing to their high defect tolerance, low defect formation energies, compositional and optical bandgap flexibility, and light/electric pulse induced stimulation possibilities.[4–10] The key processes, such as hysteresis, defect formation, and non-radiative recombination, which are detrimental to photovoltaic application act as favorable characteristics for the neuromorphic synaptic devices. Recently, methylammonium lead triiodide ($MAPbI_3$) based synaptic devices exhibiting synaptic behaviors concerning photonic and electronic stimulations were reported.[5,6,10,11] However, due to the unfavorable intrinsic phase transition and poor thin film surface morphology, very few attempts were made with formamidinium cation-based perovskites for their neuromorphic properties.

To overcome these limitations a light-triggered MA-doped $FAPbI_3$-based neuromorphic device was reported to demonstrate the possibilities in biomimicking synaptic functions

D. S. Assi, V. Karthikeyan, V. A. L. Roy
Electronics and Nanoscale Engineering
James Watt School of Engineering
University of Glasgow
Glasgow G12 8QQ, UK
E-mail: Vaithinathan.Karthikeyan@glasgow.ac.uk;
Roy.Vellaisamy@glasgow.ac.uk

The ORCID identification number(s) for the author(s) of this article can be found under https://doi.org/10.1002/aelm.202300285

M. P. Haris, S. Kazim, S. Ahmad
BCMaterials
Basque Center for Materials
Applications
and Nanostructures
UPV/EHU Science Park
Leioa 48940, Spain
E-mail: shahzada.ahmad@bcmaterials.net

S. Kazim, S. Ahmad
IKERBASQUE
Basque Foundation for Science
Bilbao 48009, Spain

V. A. L. Roy
School of Science and Technology
Hong Kong Metropolitan University
Ho Man Tin Hong Kong

**ADVANCED
SCIENCE NEWS**

www.advancedsciencenews.com

**ADVANCED
ELECTRONIC
MATERIALS**

www.advelectronicmat.de

including paired-pulse facilitation (PPF), excitatory post-synaptic current (I_{EPS}) with potentiation/depression functions.[12] Their light-triggered artificial synapse exhibited a dynamic response against environmental changes suggesting its applicability in perceiving environmental changes and tuning the information processing. By hybridizing the organic and inorganic cations, five significant synaptic functionalities in mixed lead halide perovskite-based memristive devices were shown.[13] However, the presence of higher trap charge states, low dielectric constant, and limited optoelectronic properties and their poor endurance reliability requires engineering in the perovskite structure to be more effective for neuromorphic applications.

With these intentions, here we developed a powdered $Cs_{0.1}FA_{0.9}PbI_3$ (CsFAPbI$_3$) with a high dielectric constant to store and transfer charges more efficiently, with low trap charge state density for a larger charge carrier lifetime leading to a larger ON/OFF ratio in memristor-based neuromorphic devices. Further, CsFAPI possesses the ability to block water molecules five times higher than FAPI$_3$, which is way higher than MAPI.[13] The enhanced optoelectronic properties in CsFAPbI$_3$ also provide advantages of photoconductive synaptic switching devices. Following this, we report the design and development of an electric-stimulated two-terminal artificial synaptic device using pre-synthesized CsFAPbI$_3$, which emulates most significant biological synaptic functionalities such as spike rate-dependent plasticity (SRDP), the transformation from short-term plasticity (STP) to long-term plasticity (LTP) with energy efficient learning-forgetting-relearning (L-F-R) process. Overall, our demonstration of neuromorphic properties in CsFAPbI$_3$ suggests that perovskite-based structures are the material of choice for large-scale and cost–effective neuromorphic devices.

2. Results and Discussion

2.1. CsFAPbI$_3$ thin Film from Polycrystal-Based Precursor

The CsFAPbI$_3$ thin films were deposited from pre-synthesized perovskite through a spin-coating technique[14,15] (detailed in the experimental section). The spin-coated thin films were further annealed at 80 °C for 30 min to ensure the perovskite phase. It is worth noting that this low-temperature processability could be adapted to realize flexible artificial synaptic devices in the future. We performed X-ray photoelectron spectroscopic studies of the perovskite thin film to identify the elemental composition. The characteristic peaks of Cs 3d$_{5/2}$ and Cs 3d$_{3/2}$ at 724.48 and 738.5 eV, respectively (**Figure 1**a), suggest the inclusion of Cs. We investigated the optical properties of CsFAPbI$_3$ thin film by ultraviolet–visible (UV–vis) absorbance and photoluminescence (PL) spectroscopy (Figure 1b). The absorption onset recorded with an optical bandgap of 1.51 eV displayed a sub-bandgap edge indicating in-gap defect sites (Figure 1b and Figure S1, Supporting Information). However, these non-radiative recombination sites can be useful for the synaptic application contrary to their detrimental effect in photovoltaic applications.[16] The steady-state PL emission was recorded at 810 nm with a 10 nm stoke shift (Figure 1b). The structural and phase purity of the perovskite layers is critical in delivering reliable synaptic functionality and device stability. The diffractogram from the powder X-ray diffraction technique (Figure 1c), depicts the in-

tense peaks corresponding to the perovskite phase, and the absence of non-perovskite and PbI$_2$ traces affirms the high crystallinity and phase purity of fabricated thin film. Moreover, the topological morphology is deduced from scanning electron microscopy (SEM) in Figure 1d. Altogether, structural-spectroscopic microstructure investigation substantiates a phase pure, highly crystalline, homogenous CsFAPbI$_3$ thin film. We further fabricated the neuromorphic devices and probed their synaptic functionalities.

2.2. Synaptic Switching Mechanism

We investigated the synaptic switching characteristics of the CsFAPbI$_3$ memristive device with an applied potential to the presynaptic electrode to elucidate their switching mechanism and electrical charge transport properties. **Figure 2**a demonstrates the non-volatile memory characteristics with an ultralow threshold voltage (V_{SET}) of 0.28 V. At room temperature, the device displays consistent and reproducible bistable resistive switching properties. Initially, the synaptic memory cells are in a high resistance state (OFF state), under an applied threshold potential the transition process from HRS to LRS involving different conduction mechanisms occurs. We noted four different distinguished regions illustrating the transition (Figure 2b).

Region A demonstrates the phenomenon of the Thermionic Emission Limited Conduction (TELC) mechanism at a low voltage range exhibiting a linear relationship between Ln(I) and $V^{1/2}$, following the relation in equation (1), where I, q, k, ϵ, T, ϕ, T, E_e represents respectively current, electronic charge, Boltzmann's constant, dielectric permittivity, applied voltage, barrier height, absolute temperature and activation energy of electrons.[17,18]

$$I \propto A * T^2 \exp\left[-\frac{q\phi_0}{kT} + q\left(\frac{q^3 V}{4\pi\epsilon}\right)^{\frac{1}{2}}\right] \tag{1}$$

Through thermal activation by the TELC mechanism, charge carriers from the presynaptic electrode get injected into the perovskite thin film under the influence of applied electric potential. Figure 2d illustrates the characteristic ohmic conduction mechanism in Region B following equation (2).[18]

$$I \propto V \exp\frac{(-\Delta E_\epsilon)}{kT} \tag{2}$$

Following Child's law (equation 3), the charge carriers injected into the perovskite thin film induces the Space-Charge Limited-Current (SCLC) as shown in Figure 2e.[18]

$$I \propto V^\alpha \tag{3}$$

Finally, holding the charge carries in an active layer corresponding to Trapped Charge Limited Current (TCLC) model. The results derived from region C and D provide evidence that the primary mechanism of our developed synaptic device involving trapping and de-trapping charges in the grain boundaries of the perovskite thin film are induced.[18] The electrical charges gradually fill the traps between the presynaptic and postsynaptic electrodes acting as a capacitor model. As a result, the charge mobility also
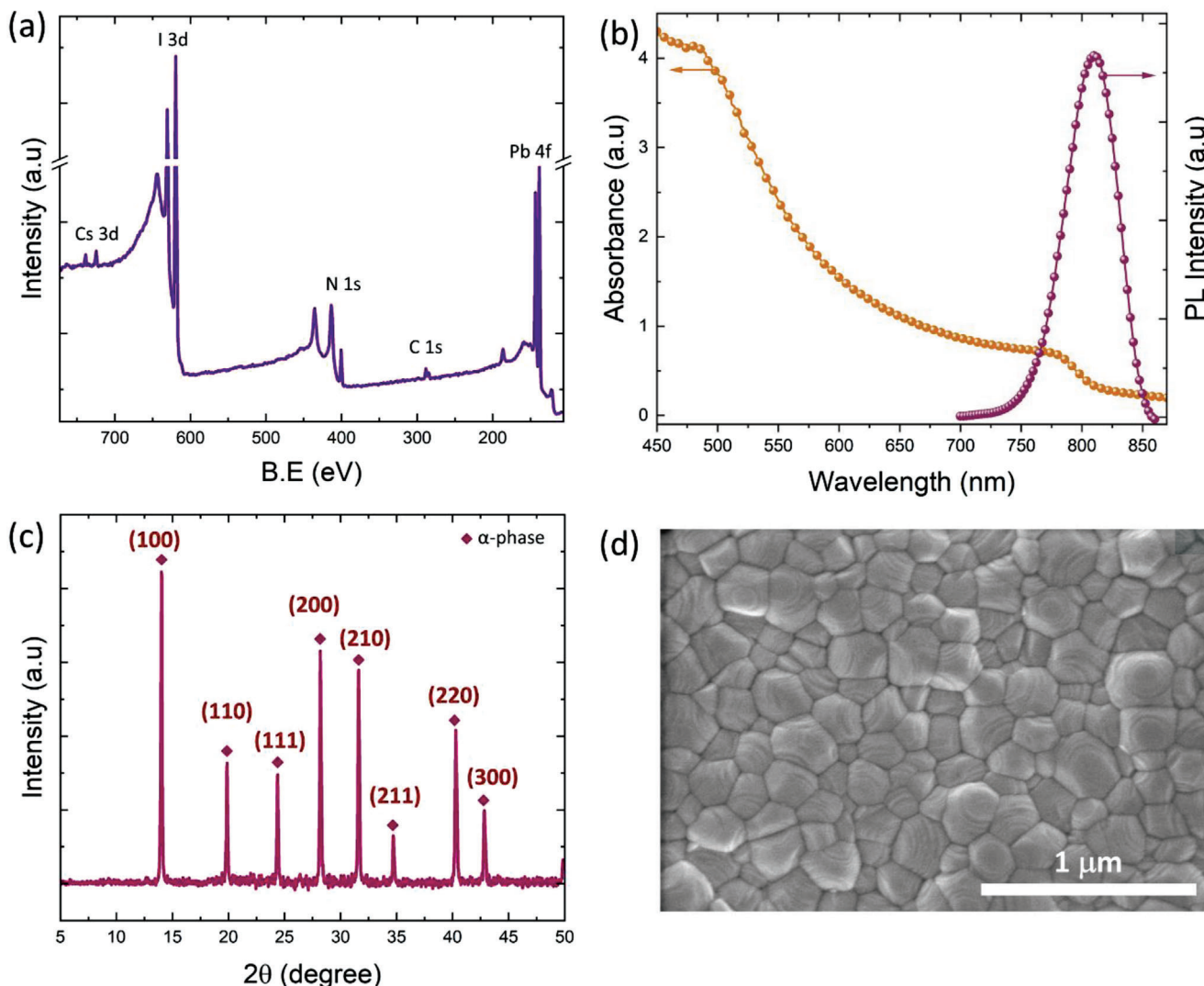
**ADVANCED
SCIENCE NEWS**

www.advancedsciencenews.com

**ADVANCED
ELECTRONIC
MATERIALS**
Open Access

www.advelectronicmat.de

Figure 1. CsFAPbI$_3$ thin film characterization: a) XPS survey spectrum indicating the presence of composite elements, b) UV–vis absorption and steady-state PL spectra, c) PXRD diffractogram indicating the phase purity and high crystallinity, and d) SEM surface morphology of the thin film.

progressively increases causing a transition to the LRS state. The conduction mechanisms in our fabricated device are an exact imitation of biological synaptic behavior in the human brain which vouches for them being exceptional for realizing neuromorphic bioelectronic devices.

2.3. Neuromorphic Properties

Biologically, synapses are the basic unit of the human neural system responsible for the transmission of chemical signals between neurons. In a chemical synapse signal, the core elements are neurotransmitters, which are released between the synaptic cleft. When an action potential arrives at the presynaptic terminal, the membrane potential is changed, resulting in the flow of Ca^{2+} messengers in the channels between the presynaptic and postsynaptic neurons.[19,20] Similarly, emulating these synaptic behaviors, with Cs$_{0.1}$FA$_{0.9}$PbI$_3$ (CsFAPbI$_3$)

synaptic device the Ag top electrode acts as the presynaptic neuron and FTO coated-glass bottom electrode as the postsynaptic neuron. The change in conductance for an applied potential in the device's active layer causes fluctuation in synaptic weight between the presynaptic and postsynaptic electrodes. Therefore, via activating memory behavior and analog modulation of synaptic plasticity through the applied potential we can emulate the biological synaptic functions in our artificial synaptic devices.

Following the Hebbian synaptic principle, we investigate the training and learning operations of CsFAPbI$_3$ devices to decipher, the characteristic biologically plausible emulation of synaptic behaviors. Learning functions play a crucial role in the emulation process of synaptic behaviors based on spike-based computations.[21–24] Spike time-dependent plasticity (STDP) and SRDP are two major approaches for the generation of the Hebbian synaptic plasticity in the neocortex and mammalian hippocampus. The SRDP is a more realistic approach to emulating
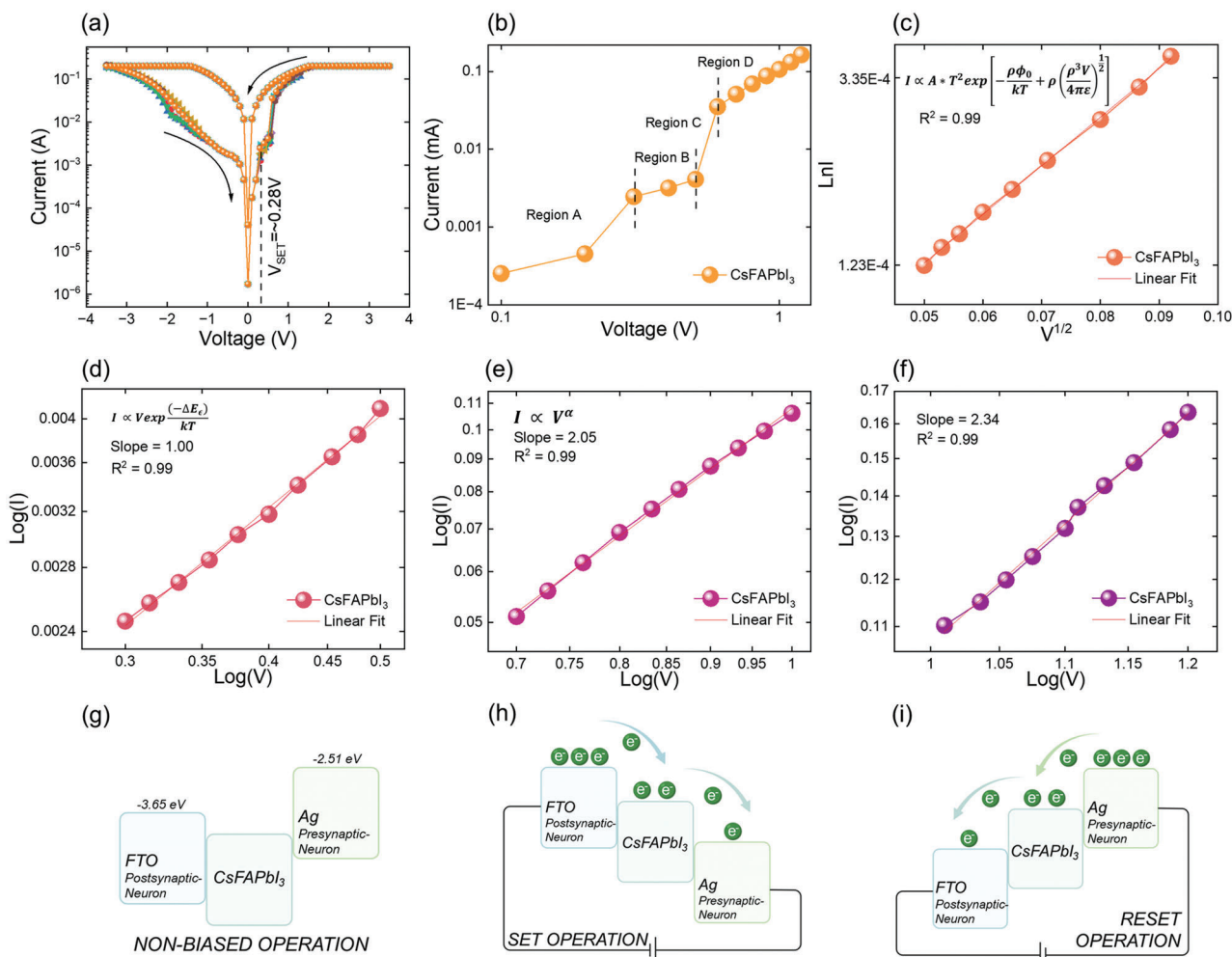
**ADVANCED
SCIENCE NEWS**

www.advancedsciencenews.com

**ADVANCED
ELECTRONIC
MATERIALS**
Open Access

www.advelectronicmat.de

Figure 2. Synaptic switching mechanism. a) Synaptic switching characteristics of our perovskite-based neuromorphic device b) Illustration of different conduction mechanism regions in the switching process. c) Thermionic Emission Limited Conduction mechanism (TELC) d) Ohmic Conduction mechanism (OC) e) Space Charge Limited Current mechanism (SCLC) f) Trapped Charged Limited Current (TCLC) g) Energy diagram of our synaptic device g) under non-biased operation. h) under SET operation i) under RESET operation.

the human neural network compared to STDP due to the random nature of the input/output spike rate. In brain cognitive behaviors, the SRDP, also termed spike-driven rate-based plasticity, is a crucial synaptic learning mechanism since the transfer of information in biological neural networks is directly connected to the average action potential firing rate.[25,26] To deeply investigate the SRDP learning rule and verify the effect of presynaptic spiking rate, consecutive spike pulse trains with a fixed amplitude (200 mV) and width (100 ms) were applied to the synaptic device with the following intervals of 10, 50, 100, 200, 500, and 1000 ms. Initially, the devices are in an HRS state during the measurement to minimize current and reduce power consumption. **Figure 3**a demonstrates the excitatory postsynaptic current (EPSC) response to 10 consecutive presynaptic stimuli with intervals ranging from 10 ms to 1 s. The gradual change of the device conductance is observed that corresponds to the modification of synaptic weight between the devices. When a shorter pulse interval is applied, the device conductance is noted to gradually increase due to the accumulation of charges in the active layer. After the pulse intervals are increased to 500 and 1000 ms, the synaptic weight of the presented synaptic device is almost negligible for facilitation. The synaptic strength efficiency between presynaptic and postsynaptic electrodes for the different pulse intervals is presented in Figure 3b. This behavior indicates the successful emulation of the SRDP behavior of the biological synapse, suggesting the dependency of the presynaptic spiking rate on the strength of synaptic plasticity. The mechanism behind this emulation process is due to the subsequent trapping of charges within the grain boundaries of the active layer perovskite thin film. Usually, during the relaxation period, the device returns to its initial state gradually due to the decreased carrier lifetimes in the active layer. When the next spike pulse is applied to the device within a short interval, the charges trapped in the active layer accumulate between the presynaptic electrodes. Subsequently, these electrical charges that are accumulated accelerate the overall conductance of the synaptic device.
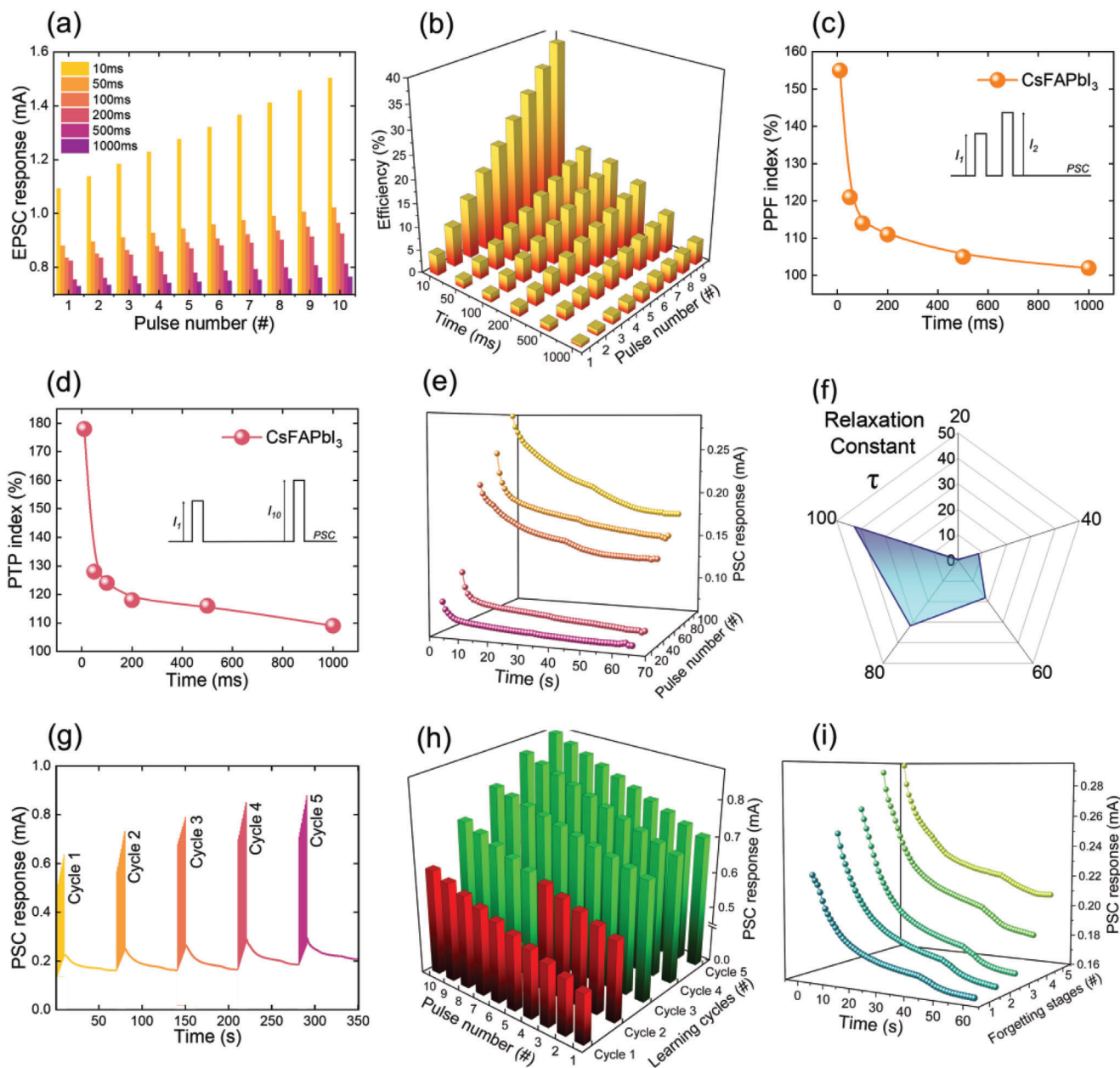
2300285 (4 of 9)

ADVANCED
SCIENCE NEWS

www.advancedsciencenews.com

ADVANCED
ELECTRONIC
MATERIALS
Open Access

www.advelectronicmat.de

Figure 3. Artificial synaptic device characteristics a) Excitatory postsynaptic current response to a series of 10 consecutive electrical pulses with varying interval times ranging from 10 ms to 1 s, b) Synaptic plasticity efficiency for different pulse intervals (from 10 ms to 1 s), c) Emulation of Paired-Pulse Facilitation (PPF) functions as a function of pulse interval, d) The representation of the Post tetanic Potentiation (PTP) function is based on pulse interval, e) The transformation process from Short-Term Plasticity (STP) to long-term plasticity (LTP), f) The relaxation constant was determined for various pulse cycles during the transition process from STP to LTP, g) Postsynaptic current response during the Learning-Relearning-Forgetting (L-R-F) emulation, h) Postsynaptic current representation of learning and relearning cycles during memorization events, and i) Postsynaptic current response level during forgetting stages every each pulse cycle.

The emulation of the Paired-Pulse Facilitation (PPF) function (Figure 3c), also known as neural facilitation, is a short-term activity-dependent form of synaptic plasticity. This process enhances the synaptic conduction instantly, amplifying the synaptic response for the second pulse.[27–31] The PPF properties are deeply analyzed by applying a pair of presynaptic pulse stimuli having different pulse intervals. The PPF index (facilitation ratio) provides a quantitative measure of short-term synaptic efficiency

following Equation (4), where A_1 and A_2 factors represent the first and second EPSC responses.

$$PPF\ index\ =\ 100\%\ \times\ \frac{A_2}{A_1} \qquad (4)$$

During the measurement, the fixed amplitude (200 mV) and width (100 ms) were applied to the synaptic device with the

**ADVANCED
SCIENCE NEWS**

www.advancedsciencenews.com

**ADVANCED
ELECTRONIC
MATERIALS**

www.advelectronicmat.de

following intervals 10, 50, 100, 200, 500, and 1000 ms. Expectedly, when the paired pulse triggers the artificial synapse, the second pulse in the postsynaptic electrode is much stronger compared to the first pulse. It can be deduced that the significant change in postsynaptic current is induced by pulses with shorter intervals. Due to frequent intervals, the electrical charges are trapped in the active layer resulting in the formation of a conduction path. The PTP function (Figure 3d) illustrates an alternative manifestation of short-term dependent plasticity that is quantified to assess short-term plasticity and learning functions.[32] The PTP properties are investigated by applying ten consecutive presynaptic pulses having different pulse intervals. The efficiency of the Post-Tetanic Potentiation is expressed through the PTP index, which represents the ratio between the response to the last pulse (A_{10}) and the initial one (A_1), as defined by formula (5).

$$PTP\ index\ =\ 100\%\ \times\ \frac{A10}{A_1} \tag{5}$$

The postsynaptic current response also significantly increases following the mechanism as in the PFF function.

In the human neural network, synaptic plasticity can be classified as STP or LTP based on retention time duration. The LTP is mainly responsible for controlling neuronal plasticity, learning, and memory operation, whereas STP focuses on data processing, decoding information, and synaptic calculations. The STP is a temporal process of strengthening the synaptic connection between the presynaptic and postsynaptic neurons with a retention time of around a few seconds. Contrary, the LTP reflects the long-lasting strengthening of the synaptic connection between neurons, maintaining a relatively long retention time compared to STP. [33–36] To evaluate these synaptic functions, the synaptic weight has to be determined to classify the strength of the synaptic connection. The direct transformation from STP to LTP is possible throughout the rehearsal events, determined by the consecutive application of the different number of spike pulses into the presynaptic neuron. During the measurement, the application of the pulses follows 20, 40, 60, 80, and 100 cycles. The postsynaptic current response as a function of decay time is (Figure 3e) which concludes that the decay rate is significantly faster in the first section indicating the relaxation time of the STP process. To fully investigate the memory transition from the STP to LTP in our device, we used the exponential equation (6) as a forgetting function in psychology to analyze the decay process and to extract the relaxation time.[37]

$$I = I_0 + Aexp\left(-\frac{t}{\tau}\right) \tag{6}$$

Here, I is a weighted current at time t, A is a perfector of the equation, τ is the relaxation constant measuring the decay rate and I_0 is a current constant. Figure 3f shows the relaxation constant τ versus the number of applied pulses to the synaptic device where we noted that with the increasing number of pulses from 20–100, the relaxation constant also increases. The results demonstrate a successful transformation from STP to LTP due to the repeated training process and learning operations.

Learning, memorizing, and forgetting behaviors are the most significant psychological functions of the human brain, which are classified as a type of empirical behavior. These functions are directly influenced by the adaptation of the biological neural net-

work to the surrounding environment and day-to-day activities. However, our memory and learned information as well as gained skills are not eternal and tend to be forgotten. Thus, the relearning process is of significant benefit for memory enhancement. It simplifies the process of regaining previously thought knowledge, even if the information has been forgotten.[38–42] Figure 3g represents the five cycles of consecutive training pulses applied to the presynaptic electrode for the synaptic device. In the emulation of the learning and relearning process in our synaptic device, an increment in conductance occurs with an applied pulse stimulus. However, when the application of pulses is stopped, the decay process begins, which is defined as a forgetting process. Figure 3h demonstrates the learning and relearning cycles for devices where the first cycle is defined as the learning period (red color), which consists of the first set of training pulses applied to the presynaptic electrode. The relearning cycle begins from the second cycle and continues until the information gets fully memorized, suggesting that the entire cycle will have a greater postsynaptic current response as compared to the first cycle. The efficiency of the learning-relearning behavior's of the device is directly connected to the amount of relearning cycles necessary to fully cross the postsynaptic current level established in the learning period. We observed that our perovskite synaptic device needs only one relearning cycle to fully memorize the learning information. This efficiency increment is associated with trapped-charge limit-current (α) mechanism developed by Ag ions trap states in the perovskite layer. We uncover that the postsynaptic current response is increasing with each cycle until its level is stabilized, establishing that the information during the learning-relearning operation gets fully memorized (Figure 3i). **Table 1** represents the neuromorphic performance of perovskite-based synaptic devices and highlights the advantages of our proposed design over the state of the art.

3. Conclusion

To conclude, we developed $CsFAPbI_3$ polycrystals to achieve control growth, low-temperature processability, and large-scale synthesis, which also delivers exceptional electronic properties compared to conventional perovskite from precursor routes. The larger dielectric constant and high carrier lifetime behavior of the developed perovskite demonstrate high capacitance for charge trapping that assists in the synaptic switching characteristics at a lower threshold voltage range. Moreover, we demonstrate neuromorphic synaptic behavior for applied electric stimuli pulse trains where the paired-pulse facilitation and the transition between short-term to long-term plasticity depict extreme efficacies. We corroborated their training and learning cycle efficacies and validated that the $CsFAPbI_3$-based device can learn with only one training cycle, which is the best among currently available neuromorphic devices. Our demonstration of neuromorphic devices based on $CsFAPbI_3$ provides a deep insight into developing cost–effective, high-efficacy artificial synaptic devices for artificial intelligence applications.

4. Experimental Section

Materials: All chemicals were purchased from Sigma Aldrich and were used as received without further purification unless otherwise stated.

Table 1. Neuromorphic performance comparison of perovskite-based artificial synaptic devices..

No	Perovskite material	Three/Two terminals	Device simulation	Synaptic function	Maximum PPF index [%]	Δt [ms]	Reference
1	$CH_3NH_3PbBr_3$	Two	Electrical	PPF, STP, LTP	91	80	[43]
2	$(PEA)_2MA_{n-1}Pb_nBr3_{n+1}$	Two	Electrical	PPF, STP, LTP	121	20	[44]
3	$CsPbI_2Br$	Two	Photonic	PPF, STP, LTP, L-F-R	142	1000	[45]
4	RbCsFAMA	Two	Electrical	SRDP, PPF, LTP	45	0.1	[46]
5	$Cs_3Bi_2I_9$	Two	Electrical	PPF, LTP	29	~30	[47]
6	$(PEA)_2SnI_4$	Three	Photonic	PPF, STP, LTP	129.7	50	[48]
7	KI–MAPbI$_3$	Two	Electrical	SRDP, PPF, LTP, L-F-R	54	~2	[49]
8	$PEA_2MA_{n-1}Pb_nI_{3n+1}$	Two	Electrical	PPF, STP, LTP	135	10	[50]
9	$AgBiI_4$	Two	Electrical	PPF, LTP	30	~0.05	[51]
10	$CsPbCl_3$	Two	Photonic	PPF, STP, LTP	126	1000	[52]
11	$Cs_2AgBiBr_6$	Two	Electrical	SRDP, PPF, LTP	130	0.2	[53]
12	$CH_3NH_3PbI_3$	Two	Photonic	PPF, LTP	40	5	[54]
13	$CsPbBr_3$	Three	Photonic	SRDP, PPF, STP, LTP	130	1	[55]
14	$CsPbBr_3QD$	Three	Photonic	PPF, LTP	132	0.5	[56]
15	$CsFAPbI_3$	Two	Electrical	SRDP, PPF, PTP, STP, LTP, L-F-R	155	10	This work

Perovskite Thin Film Fabrication: CsFAPbI$_3$ perovskite powder was synthesized from[13] and employed as the starting material for the perovskite precursor solution. 1.25 M CsFAPbI$_3$ solution was prepared by dissolving 640 mg of pre-synthesized CsFAPbI$_3$ powder in a DMF: DMSO mix solvent (4:1, v/v) through overnight stirring at 50 °C on a magnetic hot plate. The clear solution was further cooled down to room temperature and filtered using a PTFE filter with 0.45 μm pore size and spin-coated in two steps: 1000 rpm for 5 s and 5000 rpm for 20 s. 100 μL chlorobenzene was dropped on the top of the spinning substrate 5 s before the end of the program. The substrates were immediately transferred to a hotplate and annealed at 80 °C for 30 min. For ease of terminology, the deposited $Cs_{0.1}FA_{0.9}PbI_3$ will be abbreviated as CsFAPbI$_3$ throughout the text.

Synaptic Device Fabrication: Our synaptic device is based on the point-to-point memristor architecture with two electrodes positioned between the CsFAPbI$_3$ thin film layer. The top electrode, which plays the role of the presynaptic neuron was deposited by the thermal evaporation technique through the shadow mask (100 nm Ag). The FTO glass is a representation of the postsynaptic neuron (bottom electrode).

Thin Film Characterization: X-ray powder diffraction pattern was collected by using a Philips X'Pert PRO automatic diffractometer operating at 40 kV and 40 mA, in a $\theta - \theta$ configuration, with a secondary monochromator with Cu Kα radiation ($\lambda = 1.5418$ Å) and a PIXcel solid-state detector (active length in 2θ 3.347°). Data were collected from 5–50° 2θ at ambient atmosphere. A 1° fixed Soller slit, and divergence slit giving a constant volume of sample illumination was used. The absorption spectrum was collected with a Varian Cary 50 UV–vis spectrophotometer, and the steady state PL measurement was made using a spectrophotometer (PerkinElmer Instrument LS55). Morphological analysis was done by a Hitachi S-4800 SEM machine. X-ray photoelectron spectroscopy (XPS) data were collected using a SPECS system (Berlin, Germany) equipped with a Phoibos 150 1D-DLD analyzer with monochromate Al Kα radiation (1486.7 eV).

Device Characterization: The resistive switching performance of the developed synaptic device was measured and analyzed with Agilent Technologies B1500A Semiconductor Device Analyzer. Moreover, the neuromorphic properties were measured for the time domain. A different pulse interval and the number of pulse repetitions were applied to the presynaptic electrode of the artificial synapse. A digital storage oscilloscope was used to record the data.

Synaptic Measurements: Spike Rate Dependent Plasticity (SRDP): To determine the SRDP, 10 consecutive presynaptic pulse stimuli were applied to the presynaptic electrode. The pulse intervals were varied from 10 ms to 1s while keeping the pulse width at 100 ms and pulse amplitude at 200 mV. The resulting excitatory postsynaptic current (EPSC) response was measured and analyzed. *Paired-Pulse Facilitation (PPF)*: To determine the PPF function, we applied two sequential train stimuli to the presynaptic electrode. The pulse intervals were varied from 10 ms to 1s while keeping the pulse width at 100 ms and pulse amplitude at 200 mV. The PPF index was calculated using the following formula: $PPF_{index} = A2/A1$, where A1 and A2 represent the post-synaptic current (PSC) responses of the first and second pulse. *Post-Tetanic Potentiation (PTP)*: To determine the PTP function, ten sequential train stimuli were applied to the presynaptic electrode. The pulse intervals were varied from 10 ms to 1s while keeping the pulse width at 100 ms and pulse amplitude at 200 mV. The PTP index was calculated using the following formula: $PTP_{index} = A10/A1$, where A1 and A10 represent the post-synaptic current (PSC) responses of the first and last pulse. *Transition process from Short-Term Potentiation (STP) to Long-Term Potentiation (LTP)*: To determine the transition process, a group of sequential train stimuli (20, 40, 60, 80, and 100 pulses) was applied to the presynaptic electrode. The pulse width was fixed at 100 ms and the pulse amplitude at 200 mV. The results obtained were analyzed and fitted using an exponential equation commonly used as a forgetting function in psychology ($I = I_0 + A^* e^(-t/\tau)$). In this equation, I_0 represents a constant current, A represents a constant amplitude, and τ measures the relaxation constant, which reflects the rate of decay and is the value of interest. *Learning-Forgetting-Relearning process (L-F-R)*: To determine the L-F-R process, a series of five cycles of train stimuli, each consisting of 20 pulses, were administered to the presynaptic neuron. The pulse width was fixed at 100 ms and the pulse amplitude at 200 mV. The first cycle was assigned as the memorization stage, while the subsequent cycles were regarded as relearning stages. After each cycle, a natural relaxation decay known as "τ" occurred, which is commonly known as the forgetting stage.[57]

Supporting Information

Supporting Information is available from the Wiley Online Library or from the author.

Conflict of Interest

The authors declare no conflict of interest.

Author Contributions

D.S.A., V.K. - Fabrication of the device, Electrical characterization, Neuromorphic characterization, Writing-Original Draft. M.P.U.H – Material synthesis, Material characterization V.A.L.R., S.A., S.K.- Conceptualization, Supervision, Funding Acquisition, Project administration, Writing-Review & Editing.

Data Availability Statement

The data that support the findings of this study are available from the corresponding author upon reasonable request.

[1] I. H. Im, S. J. Kim, J. H. Baek, K. J. Kwak, T. H. Lee, J. W. Yang, D. E. Lee, J. Y. Kim, H. R. Kwon, D. Y. Heo, S. Y. Kim, H. W. Jang, *Adv. Funct. Mater.* **2023**, *33*, 2211358.

[2] S. G. Kim, Q. Van Le, J. S. Han, H. Kim, M.-J. Choi, S. A. Lee, T. L. Kim, S. B. Kim, S. Y. Kim, H. W. Jang, *Adv. Funct. Mater.* **2019**, *29*, 1906686.

[3] X. Xiao, J. Hu, S. Tang, K. Yan, B. Gao, H. Chen, D. Zou, *Adv. Mater. Technol.* **2020**, *5*, 1900914.

[4] R. A. John, N. Yantara, Y. F. Ng, G. Narasimman, E. Mosconi, D. Meggiolaro, M. R. Kulkarni, P. K. Gopalakrishnan, C. A. Nguyen, F. de Angelis, S. G. Mhaisalkar, A. Basu, N. Mathews, *Adv. Mater.* **2018**, *30*, 1805454.

[5] W. Huang, P. Hang, Y. Wang, K. Wang, S. Han, Z. Chen, W. Peng, Y. Zhu, M. Xu, Y. Zhang, Y. Fang, X. Yu, D. Yang, X. Pi, *Nano Energy* **2020**, *73*, 104790.

[6] X. Liu, S. Huang, K. Wang, Y. Wang, L. Yin, D. Yang, X. Pi, *Adv. Funct. Mater.* **2023**, *33*, 2211394.

[7] D. Hao, Z. Yang, J. Huang, F. Shan, *Adv. Funct. Mater.* **2023**, *33*, 2211467.

[8] R. A. John, A. Milozzi, S. Tsarev, R. Brönnimann, S. C. Boehme, E. Wu, I. Shorubalko, M. Kovalenko, D. Ielmini, *Sci. Adv.* **2022**, *8*, eade0072.

[9] J. Gong, H. Yu, X. Zhou, H. Wei, M. Ma, H. Han, S. Zhang, Y. Ni, Y. Li, W. Xu, *Adv. Funct. Mater.* **2020**, *30*, 2005413.

[10] P. Zawal, T. Mazur, M. Lis, A. Chiolerio, K. Szaciłowski, *Adv. Electron. Mater.* **2022**, *8*, 2100838.

[11] J. Liu, J. Gong, H. Wei, Y. Li, H. Wu, C. Jiang, Y. Li, W. Xu, *Nat. Commun.* **2022**, *13*, 7427.

[12] J. Gong, H. Wei, Y. Ni, S. Zhang, Y. Du, W. Xu, *Materials Today Physics* **2021**, *21*, 100540.

[13] M. P. U. Haris, J. Xia, S. Kazim, Z. Molenda, L. Hirsch, T. Buffeteau, D. M. Bassani, M. K. Nazeeruddin, S. Ahmad, *Cell Reports Physical Science* **2023**, *4*, 101304.

[14] N. Klipfel, M. P. U. Haris, S. Kazim, A. A. Sutanto, N. Shibayama, H. Kanda, A. M. Asiri, C. Momblona, S. Ahmad, M. K. Nazeeruddin, *J Mater Chem C Mater* **2022**, *10*, 10075.

[15] M. P. U. Haris, S. Kazim, S. Ahmad, *ACS Appl. Energy Mater.* **2021**, *4*, 2600.

[16] C. Zhang, S. Mahadevan, J. Yuan, J. K. W. Ho, Y. Gao, W. Liu, H. Zhong, H. Yan, Y. Zou, S. W. Tsang, S. K. So, *ACS Energy Lett.* **2022**, *7*, 1971.

[17] F. Zahoor, T. Z. Azni Zulkifli, F. A. Khanday, *Nanoscale Res. Lett.* **2020**, *15*, 90.

[18] S. R. Zhang, S. Zhou, J. Y. Mao, Y. Ren, J. Q. Yang, G. H. Yang, X. Zhu, S. T. Han, V. A. L. Roy, Y. Zhou, *Adv. Mater. Technol.* **2019**, *4*, 1800342.

[19] L. F. Reichardt, R. B. Kelly, *Annu. Rev. Biochem.* **1983**, *52*, 871.

[20] L. Squire, D. Berg, F. E. Bloom, S. du Lac, A. Ghosh, N. C. Spitzer, L. R. Squire, *Fundamental Neuroscience*, 3rd Ed, Academic Press, Cambridge, **2008**.

[21] M. Y. Tsai, K. C. Lee, C. Y. Lin, Y. M. Chang, K. Watanabe, T. Taniguchi, C. H. Ho, C. H. Lien, P. W. Chiu, Y. F. Lin, *Adv. Funct. Mater.* **2021**, *31*, 2105345.

[22] L. Yuan, S. Liu, W. Chen, F. Fan, G. Liu, *Adv. Electron. Mater.* **2021**, *7*, 2100432.

[23] H. Bian, Y. Y. Goh, Y. Liu, H. Ling, L. Xie, X. Liu, *Adv. Mater.* **2021**, *33*, 2006469.

[24] Y. Lee, J. Y. Oh, T. W. Lee, *Adv. Mater. Technol.* **2022**, *7*, 2200193.

[25] X. Wang, Y. Zong, D. Liu, J. Yang, Z. Wei, *Adv. Funct. Mater.* **2023**, *33*, 2213894.

[26] G. Lee, J. H. Baek, F. Ren, S. J. Pearton, G. H. Lee, J. Kim, *Small* **2021**, *17*, 2100640.

[27] S. Ling, C. Zhang, C. Ma, Y. Li, Q. Zhang, *Adv. Funct. Mater.* **2023**, *33*, 2208320.

[28] H. Lee, M. Jin, H. J. Na, C. Im, J. H. Lee, J. Kim, Y. J. Gong, C. Lee, E. Lee, Y. S. Kim, *Adv. Funct. Mater.* **2022**, *32*, 2110591.

[29] C. Han, X. Han, J. Han, M. He, S. Peng, C. Zhang, X. Liu, J. Gou, J. Wang, *Adv. Funct. Mater.* **2022**, *32*, 2113053.

[30] Y. Hu, M. Dai, W. Feng, X. Zhang, F. Gao, S. Zhang, B. Tan, J. Zhang, Y. Shuai, Y. Q. Fu, P. A. Hu, *Adv. Mater.* **2021**, *33*, 2104960.

[31] N. Ilyas, J. Wang, C. Li, D. Li, H. Fu, D. Gu, X. Jiang, F. Liu, Y. Jiang, W. Li, *Adv. Funct. Mater.* **2022**, *32*, 2110976.

[32] X. Wang, B. Wang, Q. Zhang, Y. Sun, E. Wang, H. Luo, Y. Wu, L. Gu, H. Li, K. Liu, *Adv. Mater.* **2021**, *33*, 2102435.

[33] C. Ban, Z. Zhang, C. Song, H. Zhang, X. Luo, X. Wang, J. Liu, Z. Liu, W. Huang, *Adv. Mater. Technol.* **2022**, *8*, 2200870.

[34] Y. Wang, L. Yin, W. Huang, Y. Li, S. Huang, Y. Zhu, D. Yang, X. Pi, *Advanced Intelligent Systems* **2021**, *3*, 2000099.

[35] G. Ding, B. Yang, K. Zhou, C. Zhang, Y. Wang, J.-Q. Yang, S.-T. Han, Y. Zhai, V. A. L. Roy, Y. Zhou, *Adv. Electron. Mater.* **2020**, *6*, 1900978.

[36] L. Yin, R. Cheng, Y. Wen, C. Liu, J. He, *Adv. Mater.* **2021**, *33*, 2007081.

[37] S. Li, F. Zeng, C. Chen, H. Liu, G. Tang, S. Gao, C. Song, Y. Lin, F. Pan, D. Guo, *J Mater Chem C Mater* **2013**, *1*, 5292.

[38] W. C. Yang, Y. C. Lin, S. Inagaki, H. Shimizu, E. Ercan, L. C. Hsu, C. C. Chueh, T. Higashihara, W. C. Chen, *Adv. Sci.* **2022**, *9*, 2105190.

[39] P. Lei, H. Duan, L. Qin, X. Wei, R. Tao, Z. Wang, F. Guo, M. Song, W. Jie, J. Hao, *Adv. Funct. Mater.* **2022**, *32*, 2201276.

[40] D. Hao, D. Liu, J. Zhang, Y. Wang, J. Huang, *Adv. Mater. Technol.* **2021**, *6*, 2100678.

[41] Y. Li, J. Wang, Q. Yang, G. Shen, *Adv. Sci.* **2022**, *9*, 2202123.

**ADVANCED
SCIENCE NEWS**

www.advancedsciencenews.com

**ADVANCED
ELECTRONIC
MATERIALS**

www.advelectronicmat.de

[42] H. L. Park, Y. Lee, N. Kim, D. G. Seo, G. T. Go, T. W. Lee, *Adv. Mater.* **2020**, *32*, 1903558.

[43] W. Xu, H. Cho, Y. H. Kim, Y. T. Kim, C. Wolf, C. G. Park, T. W. Lee, *Adv. Mater.* **2016**, *28*, 5916.

[44] S. Il Kim, Y. Lee, M. H. Park, G. T. Go, Y. H. Kim, W. Xu, H. D. Lee, H. Kim, D. G. Seo, W. Lee, T. W. Lee, *Adv. Electron. Mater.* **2019**, *5*, 1900008.

[45] S. Zhang, Y. Zhao, Q. Chen, Y. Wang, J. Jiang, Y. Wang, Y. Fu, Q. Liu, Q. Wang, D. He, *Microelectron. Eng.* **2023**, *274*, 111982.

[46] M. Loizos, K. Rogdakis, E. Kymakis, *Discov Mater* **2022**, *2*, 11.

[47] F. Luo, Y. Wu, J. Tong, F. Tian, X. Zhang, *Nano Res.* **2023**, 1, https://doi.org/10.1007/s12274-023-5411-x.

[48] Y. Sun, L. Qian, D. Xie, Y. Lin, M. Sun, W. Li, L. Ding, T. Ren, T. Palacios, *Adv. Funct. Mater.* **2019**, *29*, 1902538.

[49] J. Lao, W. Xu, C. Jiang, N. Zhong, B. Tian, H. Lin, C. Luo, J. Travas-Sejdic, H. Peng, C. G. Duan, *Adv. Electron. Mater.* **2021**, *7*, 2100291.

[50] S. J. Kim, T. H. Lee, J. M. Yang, J. W. Yang, Y. J. Lee, M. J. Choi, S. A. Lee, J. M. Suh, K. J. Kwak, *Mater. Today* **2022**, *52*, 19.

[51] H. Ye, Z. Liu, H. Han, T. Shi, G. Liao, *Mater Adv* **2022**, *3*, 7248.

[52] L. Yang, M. Singh, S. W. Shen, K. Y. Chih, S. W. Liu, C. I. Wu, C. W. Chu, H. W. Lin, *Adv. Funct. Mater.* **2021**, *31*, 2008259.

[53] J. Lao, W. Xu, C. Jiang, N. Zhong, B. Tian, H. Lin, C. Luo, J. Travas-Sejdic, H. Peng, C. G. Duan, *J Mater Chem C Mater* **2021**, *9*, 5706.

[54] X. Zhu, W. D. Lu, *ACS Nano* **2018**, *12*, 1242.

[55] Y. Wang, Z. Lv, J. Chen, Z. Wang, Y. Zhou, L. Zhou, X. Chen, S. T. Han, *Adv. Mater.* **2018**, *30*, 1802883.

[56] K. Wang, S. Dai, Y. Zhao, Y. Wang, C. Liu, J. Huang, *Small* **2019**, *15*, 1900010.

[57] D. S. Assi, H. Huang, V. Karthikeyan, V. C. S. Theja, M. M. de Souza, N. Xi, W. J. Li, V. A. L. Roy, *Advance Science* **2023**, https://doi.org/10.1002/advs.202300791.

2300285 (9 of 9)